RSC Sustainability

ROYAL SOCIETY OF CHEMISTRY

PAPER

View Article Online
View Journal | View Issue

Cite this: *RSC Sustainability*, 2025, **3**, 2952

CO_2 capture by carboxylate ionic liquids: fine-tuning the performance by altering hydrogen bonding motifs†

Mohammad Yousefe, [a] Katarzyna Glińska,[a] Michael Sweeney,[b] Leila Moura, [b] Małgorzata Swadźba-Kwaśny [b] and Alberto Puga *[a]

The use of ionic liquids (ILs) for CO_2 capture has drawn significant attention due to their tuneable structural design and non-volatility. Among these, carboxylate ionic liquids, particularly in the presence of water as a hydrogen bond donor, show great promise due to their effective chemical sorption mechanism, leading to bicarbonate, and low regeneration energy requirements. The additional presence of hydroxyl groups in their structures is expected to affect both hydrogen bonding network and CO_2 capture capacity. This study systematically investigates the role of hydroxyl moieties in tetraalkylammonium cations of carboxylate ionic liquid hydrates on their physicochemical properties and CO_2 solubility. The ILs studied are based on the trimethylpropylammonium cation or choline as a hydroxyl-containing analogue, paired with either acetate or propionate. The solubilities of CO_2 in each IL at different H_2O/IL hydration ratios were determined by a headspace gas chromatography method. The effects of water, in addition to those of cationic hydroxyl, on CO_2 capture performance were evaluated. To this end, nuclear magnetic resonance and infrared spectroscopy results are presented and analyzed to propose distinct chemical sorption mechanisms in either scenario.

Received 15th February 2025
Accepted 4th June 2025

DOI: 10.1039/d5su00108k

rsc.li/rscsus

Sustainability spotlight

The rising carbon dioxide levels in the atmosphere, caused by human activities, especially the usage of fossil fuels, have brought us to a critical point. Historically, we relied on natural CO_2 sinks such as forests and oceans to absorb excess emissions. However, these natural processes are unable to keep up with the amount of anthropogenic CO_2 emissions. To avoid catastrophic effects of climate change caused by increased CO_2 concentrations in the atmosphere, implementation of carbon capture, either from point sources or directly from the atmosphere, is critical for reducing industrial emissions because technology and efficiency enhancements alone cannot eliminate CO_2 emissions completely. To attain net-zero emissions, developing environmentally friendly CO_2 capture materials with low energy penalty, such as carboxylate ionic liquid hydrates, is crucial.

Introduction

To avoid catastrophic effects of climate change caused by increased CO_2 concentrations in the atmosphere, implementation of carbon capture, either from point sources or directly from the atmosphere, is becoming crucial. The most common technology for CO_2 capture is based on amine scrubbing,[1,2] initially patented in the 1930s.[3] This method involves a reaction between aqueous amines and CO_2. Subsequently, amines are regenerated by stripping CO_2, typically at 100–120 °C, which requires substantial energy, potentially generating more CO_2 emissions.[4,5] Second-generation amines, including aqueous solutions of piperazine and other advanced amine sorbents, offer faster kinetics.[6–9] Nevertheless, all amine-based technologies suffer from oxidative degradation and equipment corrosion, which pose safety risks and necessitate infrastructure and sorbent renewal.[10–12] Due to their relatively high vapor pressure, amines tend to evaporate during the regeneration process. The need for sorbent make-up and potential release of amines to the atmosphere have negative impacts on both sustainability and cost efficiency of the process.[13] These shortcomings motivated research into alternative, chemically stable and non-volatile solvents, such as ionic liquids, that could replace amines in CO_2 capture processes.[14–17]

Ionic liquids (ILs) are salts that remain liquid at temperatures below 100 °C.[18] Conventionally, these compounds are made up entirely of cations and anions, that are typically bulky and asymmetric, thus hindering efficient packing and in turn enhancing their stability in a liquid phase at ambient temperatures. There are numerous possible combinations of cations

[a]*Department of Chemical Engineering, Universitat Rovira i Virgili, Av. Països Catalans, 26, 43007 Tarragona, Spain. E-mail: alberto.puga@urv.cat*

[b]*The QUILL Research Centre, School of Chemistry and Chemical Engineering, Queen's University of Belfast, Belfast, BT9 5AG, Northern Ireland, UK*

† Electronic supplementary information (ESI) available. See DOI: https://doi.org/10.1039/d5su00108k

and anions, resulting in high tuneability in the design of ILs. This flexibility, accompanied by negligible vapor pressure, makes ILs suitable for a wide range of applications, including gas separation.[19–22]

The poor packing of ions in the ILs results in a large free volume, which increases physical CO_2 solubility. Moreover, specific cations and anions with basic moieties can interact with CO_2 *via* chemical reactions, typically of acid–base type.[23–27] According to recent studies, ILs can compete with amine-based sorbents in terms of energy efficiency,[28] as well as capital or operating costs, for post-combustion carbon capture. Notwithstanding this, the use of IL sorbents poses concerns, mainly related to their relatively high viscosities and possibility of solids formation upon CO_2 absorption. The former issue can be partly circumvented by employing solid-supported phases, whereas the latter requires advances on molecular design. These critical challenges must be seriously considered regarding the potential use of ILs for next-generation CO_2 capture technologies.[28–30]

Choline (*i.e.* 2-hydroxyethyl(trimethyl)ammonium) is a biodegradable, inexpensive, and water-soluble organic cation. Choline chloride is recognized as an essential nutrient, and was added to the list of human vitamins (vitamin B_4) by the National Academy of Sciences in 1998.[31] Ionic liquids containing choline cations have attracted considerable interest because of their availability, low toxicity, and excellent biodegradability.[32] However, the presence of the hydroxyl group in the cation has a great influence on the physicochemical properties of choline-based ionic liquids, and hence, detailed studies are required to select suitable anions for any particular application. According to molecular dynamics simulations and experimental studies, the OH group influences CO_2 solubility in choline lactate or methylsulfate ILs, enhancing cation–anion interactions due to hydrogen bonding, in turn leading to reduction of the effective free volume for CO_2 absorption.[33–35] Moreover, the presence of OH groups on cations increases the viscosity of ILs, which has a direct effect on the kinetics of CO_2 capture.[36–38]

Notwithstanding the mentioned burdens that hydrogen bond donor moieties, such as hydroxyls, may pose to mass transfer, they also enable particular interactions with carbon dioxide. The hydroxyl group in the choline cation, when combined with appropriate anions, might offer new carbon dioxide capturing routes.[39] Bhattacharyya *et al.* demonstrated that the hydroxyl group in the cation of choline-based ILs with aprotic N-heterocyclic anions may react with CO_2 forming organic alkyl carbonic acid functionalities, in addition to carbamates, although this route would be promoted by the high basicity of the amide groups in the anions.[40] Importantly, such basic strength greatly hampers the reversal of these chemical sorption mechanisms. Such ILs with strongly basic anions require vacuum (1 mbar) for long time (3 h) for significant, albeit incomplete, desorption. This implies high energy requirements for regeneration.

Considering sorbent materials with low energy penalty in the CO_2 capture and release process, carboxylate-based ionic liquids are an attractive class of materials. The remarkably high chemisorption of CO_2 with this set of materials is based on Lewis acid–base reactivity, despite the relatively weak basicity of carboxylates.[41–44] Moreover, carboxylate IL-based materials in their hydrated form show a dramatic enhancement of CO_2 solubility due to the formation of bicarbonate in the reaction between CO_2 and water (Scheme 1).[44–50] The addition of water to the carboxylate-based ILs, results in an increase of CO_2 solubility until the optimal H_2O/IL ratio, above which CO_2 absorption capacity decreases. The maximum CO_2 solubility in a series of carboxylate-based ionic liquids was observed to be at 1 : 1 H_2O/IL molar ratio.[44–48,50–52] The presence of functional groups capable of participating in hydrogen bonding may affect CO_2 solubility, absorption enthalpy, and other physicochemical parameters such as heat capacity, density or viscosity. In this regard, the effects of hydroxyl groups in carboxylate hydrate IL systems remain largely unexplored.

In this study we explored the effect of hydration levels on the CO_2 capture capacity in two sets of carboxylate-based ILs. Primarily, the H_2O/IL molar ratio effect on CO_2 solubility in hydrated tetraalkylammonium carboxylate ILs was investigated. Furthermore, the obtained results were compared with their choline-based counterparts to understand whether the hydroxyl group on the cation can act as a hydrogen bond donor to influence chemical sorption, and to study its effect on CO_2 uptake. Therefore, trimethylpropylammonium acetate and propionate ($[N_{1\,1\,1\,3}][AcO]$ and $[N_{1\,1\,1\,3}][Pro]$, respectively) and the hydroxylated analogues choline acetate and propionate ($[N_{1\,1\,1\,2OH}][AcO]$ and $[N_{1\,1\,1\,2OH}][Pro]$, respectively) were synthesized, and their physicochemical properties measured. Moreover, their CO_2 sorption capacities (mostly in hydrated forms at different H_2O/IL molar ratios) were screened at 35 °C and 3.0 bar ± 0.1 as the initial pressure.

Materials and methods

Materials

All chemicals were used as received unless otherwise stated. Choline hydroxide solution (46% wt in H_2O), propionic acid (100%), acetic acid (100%, for HPLC), trimethylamine solution (43.0–49.0% in H_2O), and 1-bromopropane were purchased from Sigma-Aldrich. Acetonitrile (99.9%) was purchased from Labkem. Diethyl ether was obtained from Scharlab. Amberlite IRN-78 Ion exchange resin was purchased from Thermo Fisher Scientific. Carbon dioxide (99.95% purity), argon, and nitrogen gases were obtained from BOC.

Ionic liquid synthesis

The choline-based ILs were synthesized by direct anion exchange acid–base neutralization method from commercially available hydroxide solutions. As an example, aqueous choline hydroxide (46%) was added drop-wise to an equimolar amount of propionic acid in Milli-Q® water, up to a known volume, in a round bottom flask to reach the calculated final molar equivalence pH point as measured using a Metrohm pH meter to form choline propionate ($[N_{1\,1\,1\,2OH}][Pro]$).[53] Subsequently, water was removed at 60 °C under reduced pressure (reaching 10^{-3} mbar in the latter stages). The resulting orange viscous

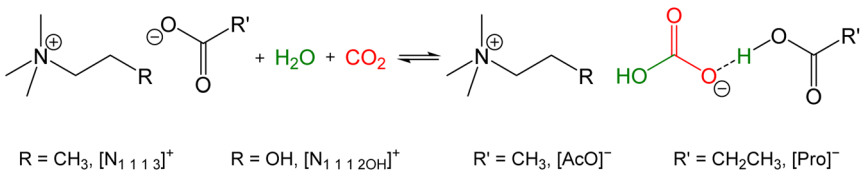

Scheme 1 Schematic reaction mechanism of CO_2 absorption by the tetraalkylammonium carboxylate ILs used in this work, in the presence of water. Cation and anion codes are indicated next to the definition of the R or R′ groups in each case.

ionic liquid was characterized by NMR confirming the expected structure and composition, and its water content was determined by the Metrohm coulometric Karl Fischer titration system (see below).

The synthesis of $[N_{1\,1\,1\,3}]^+$-based ILs was performed in three steps. Initially, trimethylamine was quaternised with 1-bromopropane, then the resulting bromide salt exchanged with hydroxide, and subsequently, anion exchange neutralization with the desired acid was performed. To prepare trimethylpropylammonium bromide, 1-bromopropane (11.6 mL, 128 mmol), trimethylamine (44.4% in H_2O, 33.5 mL, 252 mmol) and acetonitrile (50 mL) were added to a round-bottom flask. After six hours of stirring at 40 °C, the reaction mixture was cooled to room temperature. Volatiles were removed in a rotary evaporator, leaving an oily residue. Diethyl ether was added to precipitate the product, which was subsequently filtered and washed with more diethyl ether and dried under reduced pressure, leaving $[N_{1\,1\,1\,3}][Br]$ as a white solid.[54] In the second step, trimethylpropylammonium hydroxide ($[N_{1\,1\,1\,3}][OH]$) was prepared from $[N_{1\,1\,1\,3}][Br]$ using an ion-exchange resin (Amberlite IRN-78). A mixture of the resin (400 mL) and Milli-Q® water was placed in a flash chromatography column. $[N_{1\,1\,1\,3}][Br]$ (25.5 g) was dissolved in Milli-Q® water (500 mL) and passed through the resin at a rate of 1 drop every 20–30 seconds under N_2 atmosphere. The resin was subsequently washed with Milli-Q® water (0.5 L), and the aqueous effluents were mixed together to form the final solution of $[N_{1\,1\,1\,3}][OH]$. The concentration of $[N_{1\,1\,1\,3}][OH]$ was determined by titration with an aqueous HCl solution of known concentration.[53] The final $[N_{1\,1\,1\,3}][AcO]$ and $[N_{1\,1\,1\,3}][Pro]$ were synthesized similarly to the method described above for $[N_{1\,1\,1\,2OH}][Pro]$, from the generated aqueous $[N_{1\,1\,1\,3}][OH]$ solution. The purity of the ionic liquids was checked by ^1H and ^{13}C NMR in DMSO-d_6. The presence of residual halide in the aqueous phases containing the ILs was discarded based on the silver test, using acidic aqueous silver(I) nitrate (0.30 M $AgNO_3$ in 1.0 M HNO_3).

NMR and FTIR spectroscopy

The prepared ILs were analysed by ^1H and ^{13}C NMR spectroscopy on a Varian Gemini 400 spectrometer (400 MHz), either dissolved in dimethyl sulfoxide-d_6 (DMSO-d_6) or as neat ILs using DMSO-d_6 in a sealed capillary tube as an external standard. For some CO_2-saturated samples which underwent a phase change from liquid to solid, solid-state NMR experiments were conducted on a 500 MHz Bruker Avance Neo wide bore magnet equipped with a 4 mm Bruker H-F/X/Y DVT probe at 5 kHz Magic Angle Spinning (MAS). Attenuated total reflectance Fourier-transform infrared (ATR-FTIR) spectra were recorded on a PerkinElmer Spectrum 100 FT-IR spectrometer.

Thermal behaviour and stability studies

Thermal behaviour was studied by differential scanning calorimetry (DSC) on a Q2000 TA Instruments with an RCS 90 cooling system attached. The thermal program in the DSC analyses consisted of three cycles, each of them comprising a heating ramp at 5 °C min^{-1}, under N_2 (50 mL min^{-1}) up to 60 °C (for hydrated ILs) or 130 °C (for dried ILs), and a cooling ramp at 5 °C min^{-1}, under N_2 (50 mL min^{-1}) down to −80 °C (for hydrated ILs) or −90 °C (for dried ILs). The thermogram of the third cycle's heating ramp was utilized to fully process the thermal events: glass transition temperatures (at the midpoint of the mild fluctuations in heat flow, estimated ±1 °C) and melting temperatures (at the onset of the endothermic peaks, estimated ±1 °C). Thermal stability was studied by thermogravimetric analysis (TGA) on a 5500 Discovery Series TA Instruments. TGA profiles in a dynamic mode were recorded from 30 to 700 °C, at 10 °C min^{-1}, under N_2 atmosphere as balance/sample purge inert gas (50 mL min^{-1}) in an open platinum pan. The measured decomposition temperatures were approximated with an error of 1 °C.

Density and viscosity measurements

Densities and viscosities (dynamic and kinematic) of IL and hydrated IL samples were measured using the Stabinger method by SVM 3001 Anton Parr with 5 °C increments over the temperature scan range 10–70 °C (±0.005 °C).

Adjustment of H_2O/IL molar ratios

Prior to mixing the ILs with water, the ILs were vacuum-dried (60 °C, 10^{-3} mbar, 3 days) and water content was measured to be less than 300 ppm using Karl Fischer Coulometry, Metrohm 899 coulometer. To prevent CO_2 and excess H_2O absorption from the atmosphere, the ILs were hydrated by adding calculated H_2O to a Schlenk flask charged by IL and with a gentle flow of argon. Additionally, water content was remeasured using Karl Fischer Coulometry before each CO_2 solubility measurement to ensure the H_2O/IL ratio.

CO_2 absorption measurements

The CO_2 solubility measurements were performed by headspace gas chromatography (HS-GC), as a screening gas sorption method. The procedure detailed by Young *et al.*[55] is succinctly summarized as follows: The HS-GC technique determines the

concentration of dissolved gas in sorbents by measuring pressure differences in the gas phase (headspace) above the sorbents (ILs or their hydrates) before and after contact with CO_2 and equilibration. This method consists of 4 steps: sample or calibration vial preparation, pressurization, equilibration, and HS-GC measurement. Extended details of the procedure are available in the ESI.†

Known volumes (0.3–0.5 mL) of the IL or IL hydrate samples were placed in a sealed vial (20 mL), with a magnetic stirring bar under a controlled atmosphere. After evacuation, the vials were pressurized with CO_2 up to 3.0 ± 0.1 bar and allowed to equilibrate at 35 °C. The HS-GC response was determined by gas chromatography. The measured concentration in the headspace and the known volume of the liquid were used to compute gas solubilities. The CO_2 sorption measurements for each point were collected in triplicate to ensure a reliable analysis.

Results and discussion

Thermal properties of anhydrous and hydrated ILs

The addition of water to ionic liquids not only enhances CO_2 capture solubility in carboxylate-based ILs but also broadens the liquidity range of these sorbents, as shown in Table 1, and Fig. 1. Minimum IL hydration levels were chosen to maintain the samples in their liquid states, according to DSC thermographs (Table 1) and visual observations, for sorbent studies at room temperature. Initially, in order to find the minimum H_2O/IL ratio, samples of the ILs dried in Schlenk flasks under high vacuum were mixed with Milli-Q® water in 0.05 mol(H_2O)/mol(IL) increments at room temperature and the resulting mixtures were magnetically stirred. Water additions were continued until neither solids nor crystals were observed by naked eye. Analyses by Karl Fischer coulometry and DSC measurements were performed to validate the obtained results.

As illustrated in Fig. 1, the DSC thermograph of dry $[N_{1\,1\,1\,2OH}][AcO]$ shows a melting point at 88 °C upon heating and a crystallisation event at *ca.* 40 °C upon cooling. Other publications have reported lower melting temperatures, namely 72 or 51 °C.[56,57] The disagreement between different reports might be due to slightly different hydration degrees in each sample. In fact, addition of 1.25 mol(H_2O) results in a room-temperature ionic liquid hydrate, and neither melting nor crystallisation events are observed by DSC down to −80 °C (Fig. 1). This indicates a noteworthy and remarkably expanded temperature range for choline acetate hydrates, making them suitable for CO_2 capture applications typically conducted at ambient temperature. Moreover, both flue gas and atmospheric CO_2 streams generally contain water, which may compensate for any water loss during the regeneration phases. However, adjusting the CO_2 capture and release process in such a way that water levels in the hydrated ILs remain within the optimal range might prove challenging. Future work will be devoted to long-term cyclic performance tests to establish appropriate working conditions. In stark contrast to choline acetate, $[N_{1\,1\,1\,3}][AcO]$ is a solid up to temperatures in excess of 100 °C. Addition of small amounts of water also depresses melting points, resulting in room-temperature ionic liquid hydrate at equimolar hydration degree (T_m = 14 °C, Table 1) and above.

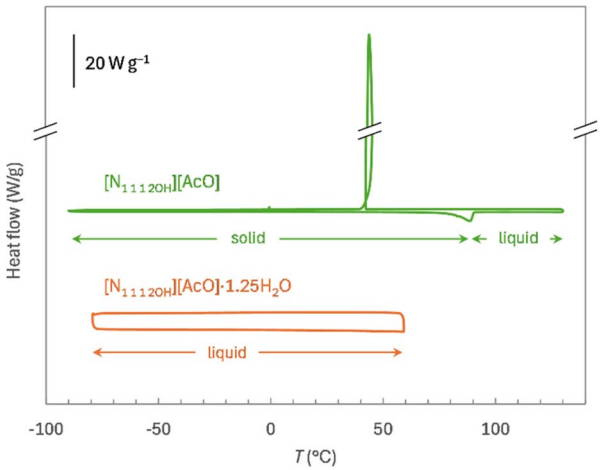

Fig. 1 Second cycle thermographs of $[N_{1\,1\,1\,2OH}][AcO]$ (green) and $[N_{1\,1\,1\,2OH}][AcO]\cdot1.25H_2O$ (orange) measured by DSC (offset along the *y* axis for clarity), showing the solid and liquid ranges for the former, delimited by the melting point (down peak at 88 °C), and the fully liquid range for the latter. Up-signals indicate exothermic events; heating/cooling rates: 5 °C min^{-1}; carrier gas: N_2 (50 mL min^{-1}).

Table 1 Thermal properties of the anhydrous or hydrated ILs[a]

IL or IL hydrate	T_g[b] (°C)	T_m[c] (°C)	T_{dec}[d] (°C)
$[N_{1\,1\,1\,2OH}][AcO]$		88	
$[N_{1\,1\,1\,2OH}][AcO]\cdot1.25H_2O$			171
$[N_{1\,1\,1\,3}][AcO]$		119	
$[N_{1\,1\,1\,3}][AcO]\cdot H_2O$		14	168
$[N_{1\,1\,1\,2OH}][Pro]$	−73		
$[N_{1\,1\,1\,2OH}][Pro]\cdot H_2O$			177
$[N_{1\,1\,1\,3}][Pro]$		44	
$[N_{1\,1\,1\,3}][Pro]\cdot1.5H_2O$		−6	163

[a] The H_2O/IL molar ratio for the hydrated ILs is the minimum leading to liquid materials at room temperature (>20 °C) showing no signs of solidification upon medium-term (several days) storage, except for $[N_{1\,1\,1\,2OH}][Pro]\cdot xH_2O$, which remains in liquid state for any hydration ratio. [b] T_g: glass transition temperature. [c] T_m: melting temperature. [d] T_{dec}: decomposition temperature, determined as the onset of weight loss above dehydration events (>150 °C) in TGA traces.

Phase behaviour of propionate ILs and their hydrates is markedly different to that of the acetates, as liquid ranges are significantly expanded. Interestingly, anhydrous choline propionate does not undergo solidification at ambient—or even deeply sub-ambient—temperatures (T_g = −73 °C, Table 1), in agreement with Ohno and co-workers.[57] Hydrated $[N_{1\,1\,1\,2OH}][Pro]$ formulations are also consistently liquid across wide temperature ranges. Replacing choline with the non-hydroxylated analogue cation leads to increased solidification tendency, although melting point is lower than that of the acetate counterpart (T_m = 44 °C for $[N_{1\,1\,1\,2OH}][Pro]$, Table 1), whereas hydration depresses the melting point slightly.

Thermal stability for the four hydrated ILs was evaluated by TGA (Fig. 2). The weight loss events observed below 150 °C are due to the removal of water, since all the samples analysed had

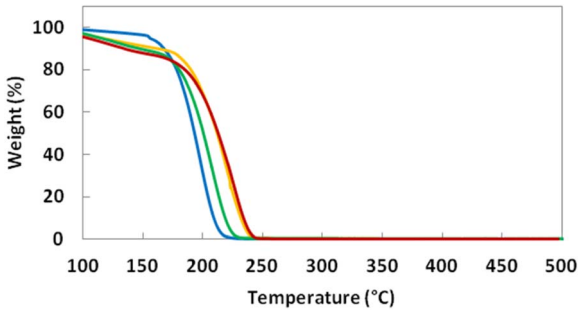

Fig. 2 Thermal decomposition curves of hydrated ILs: $[N_{1\,1\,1\,3}][Pro]$ (blue), $[N_{1\,1\,1\,2OH}][Pro]$ (orange), $[N_{1\,1\,1\,3}][AcO]$ (green) and $[N_{1\,1\,1\,2OH}][AcO]$ (red) measured by TGA. Heating rate: 10 °C min^{-1}; carrier gas: N_2, 50 mL min^{-1}.

more than 1 mol of water per mole of IL, and possibly also pre-absorbed CO_2 from the atmosphere. The decomposition temperature, determined as the onset of weight loss, of hydrated $[N_{1\,1\,1\,3}][AcO]$ and $[N_{1\,1\,1\,3}][Pro]$ occurred at temperatures below 170 °C, whereas it was slightly higher for the choline counterparts $[N_{1\,1\,1\,2OH}][Pro]$ and $[N_{1\,1\,1\,2OH}][AcO]$. These events are expected to be related to the thermal decomposition of the ammonium cations. The slight increase of the thermal stability for choline cations might be due to the presence of the hydroxyl moiety (Fig. 2 and Table 1), which would increase cation–anion interactions *via* hydrogen bonding, resulting in higher energy (higher temperature) requirement to break these interactions, in turn leading to enhancement of the overall thermal stability of the IL.

Density and viscosity

Densities and viscosities were measured for all ILs at the minimum hydration ratios at which they are fully liquid, *i.e.* $[N_{1\,1\,1\,2OH}][Pro]$, $[N_{1\,1\,1\,2OH}][AcO]\cdot 1.25H_2O$, $[N_{1\,1\,1\,3}][Pro]\cdot 1.5H_2O$ and $[N_{1\,1\,1\,3}][AcO]\cdot H_2O$ (Fig. 3 and Tables S1–S4†). Over the analysed temperature ranges, density decreases linearly with increasing temperature. As a general observation, choline-based ionic liquid materials exhibit higher densities as compared to their non-hydroxylated counterparts based on the $[N_{1\,1\,1\,3}]^+$ cation, most likely due to the heavier oxygen atom present in the hydroxyl moiety and to the more intense inter-ionic and intermolecular interactions enabled by hydrogen bonding.

The exponential decreases in viscosity observed with increasing the temperature are common for many fluids, and in particular for ionic liquids. As can be observed in Fig. 3 (bottom), the hydrated ionic liquids under study herein are moderately viscous. Their viscosities lie around 100 mPa s at room temperature, and therefore, they are reasonably fluid for the subsequent CO_2 solubility measurements described below. Conversely, the anhydrous $[N_{1\,1\,1\,2OH}][Pro]$ is a viscous liquid at room temperature (6.2 Pa s at 20 °C, Table S2†), albeit its fluidity increases markedly upon heating.

CO_2 solubility

The solubility of CO_2 in the studied ILs was measured at different hydration levels at 35 °C, and 3.0 ± 0.1 bar (initial pressure) by using the HS-GC method described in the Materials and Methods section above and in the ESI.† The results are shown in Fig. 4 and listed in Table S5.† The objective of this investigation was to screen the solubility of CO_2 at different H_2O/IL molar ratios rather than studying kinetics or determining the equilibration time required for CO_2 with ILs. Moreover, desorption and cyclic capture-release performance will be considered in future studies, encouraged by our recent results proving that CO_2 capture is readily reversible at moderate temperatures (60 °C) in carboxylate ILs.[28] To ensure that a sufficient amount of time was applied for CO_2 to reach absorption equilibrium with the ionic liquids, 72 h equilibration time was considered as a standard protocol in this work.

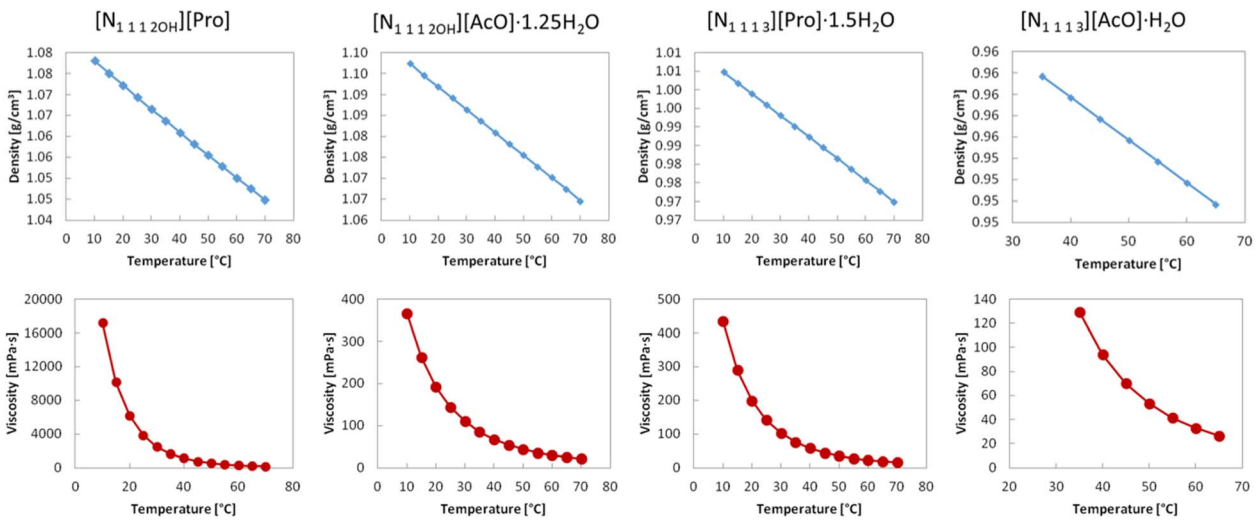

Fig. 3 Experimental densities (top) and dynamic viscosities (bottom) of $[N_{1\,1\,1\,2OH}][Pro]$, $[N_{1\,1\,1\,2OH}][AcO]\cdot 1.25H_2O$, $[N_{1\,1\,1\,3}][Pro]\cdot 1.5H_2O$ and $[N_{1\,1\,1\,3}][AcO]\cdot H_2O$ as a function of temperature.

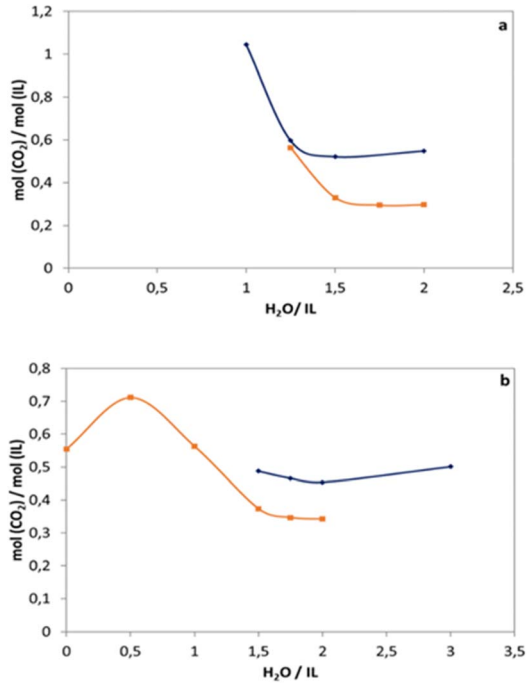

Fig. 4 Carbon dioxide uptakes, determined by GC, of mixtures of water and carboxylate ionic liquids: (a) [$N_{1\ 1\ 1\ 2OH}$][AcO] (orange, squares), and [$N_{1\ 1\ 1\ 3}$][AcO] (blue, diamonds), (b) [$N_{1\ 1\ 1\ 2OH}$][Pro] (orange, squares) and [$N_{1\ 1\ 1\ 3}$][Pro] (blue, diamonds). T = 35 °C; P(initial) = 3.0 ± 0.1 bar.

Final pressures at the end of the equilibration periods were *ca.* 2 bar.

According to the obtained results for acetate IL hydrates (Fig. 4), the solubility of CO_2 decreases with increasing the water content. In the case of [$N_{1\ 1\ 1\ 3}$][AcO], the highest CO_2 solubility was found for the lowest hydration degree for this IL, namely a 1 : 1 H_2O/IL molar ratio. Data could not be obtained for lower H_2O/IL molar ratio, because the mixture undergoes partial crystallisation below that hydration ratio at room temperature (around 20 °C). By comparing to the next point for [$N_{1\ 1\ 1\ 3}$][AcO]·1.25H_2O, the solubility of CO_2 in hydrated ionic liquid decreased by *ca.* 43%, from 1.04 to 0.59 mol(CO_2)/mol(IL). This is consistent with the 1 : 1 H_2O/IL molar ratio composition as the theoretically optimum for carbon dioxide solubility, as reported in the literature for similar carboxylate ionic liquids.[45,47,58] It is worth noting the higher than equimolar solubility of CO_2 in [$N_{1\ 1\ 1\ 3}$][AcO]·H_2O at 35 °C (1.04 mol(CO_2)/mol(IL), Table S5†), which is on a par with some of the best performing chemically absorbing, including amine-based, ILs.[59] When water is added in amounts greater than 1 : 1, it mostly functions as a diluent, saturating the coordination sphere of acetate and effectively reducing its basic strength.[44,60] As a result, formation of bicarbonate is disfavoured at higher hydration degrees, thus reducing CO_2 absorption.[45]

Regarding the hydrated [$N_{1\ 1\ 1\ 2OH}$][AcO] system, solid–liquid mixtures are formed below 1.25 mol(H_2O)/mol(IL), and therefore, measurements were carried out at higher hydration degrees. The maximum CO_2 solubility in hydrated [$N_{1\ 1\ 1\ 2OH}$][AcO] was observed for [$N_{1\ 1\ 1\ 2OH}$][AcO]·1.25H_2O, which achieved a 0.562 mol(CO_2)/mol(IL) uptake, slightly lower that the result obtained for [$N_{1\ 1\ 1\ 3}$][AcO]·1.25H_2O. Comparing [$N_{1\ 1\ 1\ 3}$][AcO] with its choline-based analogue at higher hydration degrees, the former shows better performance, that is, 0.19 and 0.25 mol(CO_2)/mol(IL) higher in CO_2 solubility for 1.5 and 2 mol(H_2O)/mol(IL) mixtures, respectively (Fig. 4). The essentially constant CO_2 absorption behaviour for H_2O/IL mixtures with hydration degrees above 1.5 mol(H_2O)/mol(IL) was observed for all of the sorbent materials tested in this work. A possible explanation to this fact might be the progressively increasing dominance of physical sorption while transitioning from a highly ionic, fairly hydrated, to a more aqueous medium.

For hydrated [$N_{1\ 1\ 1\ 3}$][Pro], no measurements were carried out below 1.45 mol(H_2O)/mol(IL), given that such mixtures undergo crystalline solids formation. Upon increasing water contents in [$N_{1\ 1\ 1\ 3}$][Pro]/H_2O, from 1.5 to 3.0 mol(H_2O)/mol(IL), CO_2 uptakes remain fairly unchanged in the range around 0.5 mol(CO_2)/mol(IL), consistent with the trend observed for acetate analogues, as discussed above, and choline prolinate. When [$N_{1\ 1\ 1\ 3}$][Pro] is compared to its hydroxylated cation analogue ([$N_{1\ 1\ 1\ 2OH}$][Pro]), a *ca.* 0.1 mol(CO_2)/mol(IL) superior performance is observed for the former, *i.e.* the non-hydroxylated IL at any of the studied hydration degrees. Notwithstanding, there is a wider CO_2 solubility measurements range in terms of water/IL molar ratios in the case [$N_{1\ 1\ 1\ 2OH}$][Pro]. As indicated above, no melting point was observed by DSC for any, including anhydrous, compositions upon cooling down to −90 °C for choline propionate (Table 1). The CO_2 solubility curve of [$N_{1\ 1\ 1\ 2OH}$][Pro]/H_2O mixtures reveals that the maximum carbon dioxide solubility is reached at a 0.5 mol(H_2O)/mol(IL) (0.711 mol(CO_2)/mol(IL)), followed by a reduction in CO_2 uptake by increasing water content (Fig. 4).

It is interesting to note that no solids were observed for choline carboxylate hydrates (namely [$N_{1\ 1\ 1\ 2OH}$][AcO] and [$N_{1\ 1\ 1\ 2OH}$][Pro]), while crystalline solids precipitated for anhydrous [$N_{1\ 1\ 1\ 2OH}$][Pro], upon CO_2 absorption. As further discussed below, the latter solidification phenomenon could be ascribed to the formation of a choline-bonded carbonate species. Conversely, the IL hydrates based on the non-hydroxylated cation namely [$N_{1\ 1\ 1\ 3}$][AcO] and [$N_{1\ 1\ 1\ 3}$][Pro]) underwent bulk solids formation after absorbing CO_2. The chemical composition of those solids was investigated by NMR and FTIR in order to complement analogous liquid-phase speciation studies, as described below.

Characterisation of IL or IL hydrates upon CO_2 uptake

Regarding anhydrous [$N_{1\ 1\ 1\ 2OH}$][Pro], which exhibits a remarkably wide liquid range across room and sub-ambient temperatures, crystals are readily formed upon exposure to carbon dioxide (see above). To assess the reactivity of CO_2 with the hydrated IL sorbent material, ^{13}C NMR measurements were performed for neat liquid samples before and after exposure to CO_2, using DMSO-d_6 in a sealed capillary tube as an external standard (Fig. 5a).

Due to the formation of solids, CO_2-saturated [$N_{1\ 1\ 1\ 2OH}$][Pro] was measured as a cloudy, albeit mostly liquid, mixture. Fig. 5a

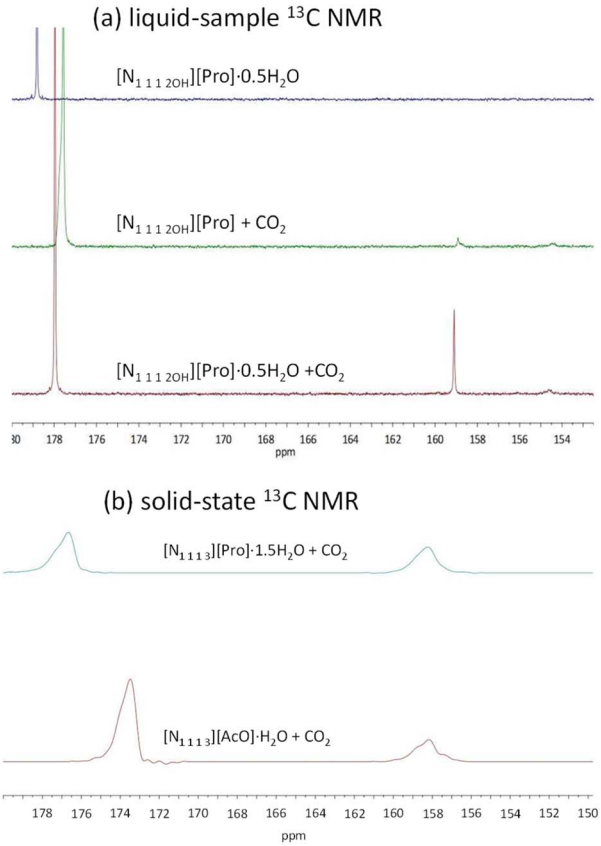

Fig. 5 (a) Liquid-sample ^{13}C NMR spectra of $[N_{1\ 1\ 1\ 2OH}][Pro]\cdot 0.5H_2O$, CO_2-saturated $[N_{1\ 1\ 1\ 2OH}][Pro]$, and CO_2-saturated $[N_{1\ 1\ 1\ 2OH}][Pro]\cdot 0.5H_2O$, using DMSO-$d_6$ in a sealed capillary tube as an external standard. (b) Solid-state magic-angle spinning (MAS) ^{13}C NMR spectra of CO_2-saturated $[N_{1\ 1\ 1\ 3}][Pro]\cdot 1.5H_2O$, and CO_2-saturated $[N_{1\ 1\ 1\ 3}][AcO]\cdot H_2O$.

shows the ^{13}C NMR spectrum with a peak at $\delta_C = 177.5$ ppm for the carboxylate carbon nucleus in the propionate anion in $[N_{1\ 1\ 1\ 2OH}][Pro]\cdot 0.5H_2O$. The ^{13}C NMR spectrum for CO_2-saturated anhydrous $[N_{1\ 1\ 1\ 2OH}][Pro]$ shows that the peak for propionate anion shifted slightly to 178.1 ppm, whereas two new weak peaks were observed at 154.8 and 159.4 ppm (Fig. 5a, middle). The latter peak, lying at a higher frequency, is consistent with the formation of bicarbonate.[45] This route is not expected to take place for anhydrous $[N_{1\ 1\ 1\ 2OH}][Pro]$ since it requires the participation of water. A plausible explanation would be that a small amount of water might have been absorbed during sample preparation, eventually leading to the formation of hydrogencarbonate.

What is interesting to note is the presence of the additional peak at 154.8 ppm. Since this peak is not observed for $[N_{1\ 1\ 1\ 2OH}][Pro]$ before contact with CO_2, the possibility of being due to an impurity is ruled out. Although the identity of the species giving rise to this peak is uncertain, the fact that it newly appeared upon CO_2 absorption peak suggests formation of another trapped CO_2 species. One possibility is the formation of an organic alkyl carbonate species on the hydroxyl group of the choline cation.[40,61] Another interesting observation

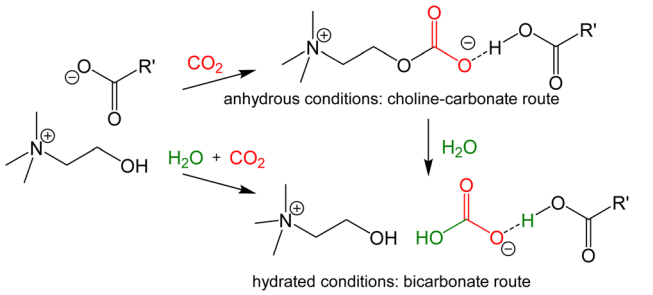

Scheme 2 Postulated reaction mechanism of CO_2 absorption in choline carboxylate ILs in the absence of water, presumably resulting in a cation-bonded organic alkyl carbonate species. In the presence of water, the known mechanism leading to bicarbonate dominates.

is related to the measurements for a hydrated sample, namely $[N_{1\ 1\ 1\ 2OH}][Pro]\cdot 0.5H_2O$, after being saturated with CO_2. The bicarbonate signal (159.6 ppm) shows noticeably higher intensity as compared to that in the anhydrous counterpart, reinforcing the above hypothesis and confirming the main expected chemical sorption mechanism. Conversely, the signal at lower frequency (higher field) is still observed at 155.3 ppm with similar intensity (Fig. 5a). Therefore, we speculate that an organic alkyl carbonate (or carbonic acid) is formed in anhydrous $[N_{1\ 1\ 1\ 2OH}][Pro]$ upon CO_2 uptake. This might take place by nucleophilic attack of the hydroxyl oxygen atom, probably partly deprotonated by the propionate anion acting as a base, to carbon dioxide. Water addition would lead to hydrolysis and subsequent bicarbonate formation (Scheme 2). Further experiments are being considered to help elucidating this proposed CO_2 capture mechanism under anhydrous conditions.

To complement the NMR results, samples of both anhydrous and hydrated $[N_{1\ 1\ 1\ 2OH}][Pro]$ were analysed by ATR-FTIR, before and after contacting with CO_2 (see Fig. S1†). The expected formation of bicarbonate in $[N_{1\ 1\ 1\ 2OH}][Pro]\cdot H_2O$ is confirmed by the emergence of the typical asymmetric stretching signal at 1636 cm^{-1} upon chemical absorption of CO_2.[28,44,45] By contrast, this signal is missing in the spectrum of the anhydrous ionic liquid, and another prominent one, presumably attributable to an organic alkyl carbonate species, is observed at 1676 cm^{-1} ($ROCO_2^-$, Fig. S1†). Confirmation of this hypothesis will be pursued by future additional structural investigations. According to a report on zwitterionic sorbents combining guanidinium and hydroxyl moieties, for anhydrous IL a downfield shift of the α-proton adjacent to the alcohol group should be expected for the emerging intramolecular alkyl carbonate.[61] However, this shift could not be readily observed by ^{1}H NMR for neither anhydrous nor hydrated $[N_{1\ 1\ 1\ 2OH}][Pro]$ after CO_2 saturation (Fig. S3†). This could be due to either the formation of a solid upon CO_2 absorption of the anhydrous IL, whose signals would be rather weak, or to overlap of the expected α-proton signal of the alkyl carbonate ($-CH_2OCO_2$) with hydrogens in the methylene unit bonded to the central nitrogen atom ($-NCH_2$, Fig. S3†).

In the case of $[N_{1\ 1\ 1\ 3}][AcO]$ and $[N_{1\ 1\ 1\ 3}][Pro]$ hydrates, no liquid-sample NMR measurements were carried out since both

H_2O/IL mixtures underwent massive sedimentation of solids upon exposure to carbon dioxide. Instead, solid-state NMR was performed to analyse the CO_2-saturated $[N_{1\,1\,1\,3}][AcO]\cdot H_2O$, and $[N_{1\,1\,1\,3}][Pro]\cdot 1.5H_2O$ (Fig. 5, S4 and S5†). The solid-state NMR spectrum for CO_2-saturated $[N_{1\,1\,1\,3}][Pro]\cdot 1.5H_2O$ and $[N_{1\,1\,1\,3}][AcO]\cdot H_2O$ (Fig. 5b) shows two peaks in the typical region for carboxylate or related groups. The peak at higher frequency corresponds to the carboxylate carbon nucleus in the propionate or acetate anion (177 and 174 ppm, respectively), while the peak at lower frequency, is consistent with the formation of hydrogencarbonate, as expected. This confirms that the bulk solid formed upon CO_2 uptake by non-hydroxylated IL hydrates is mostly bicarbonate. This is further supported by ATR-FTIR results, which indicate the emergence of the typical bicarbonate signal (marked as $HOCO_2^-$ in Fig. S2†) in the spectrum of the solid–liquid mixture resulting after CO_2 absorption in $[N_{1\,1\,1\,3}][Pro]\cdot 1.5H_2O$.

Conclusions

The effect of hydration levels on physicochemical properties and CO_2 solubility for two sets of carboxylate (acetate or propionate) ionic liquids based on the trimethylpropylammonium cation ($[N_{1\,1\,1\,3}]^+$) or its hydroxylated analogue, that is, choline ($[N_{1\,1\,1\,2OH}]^+$), were investigated. As dehydrated, the salts are relatively low-melting solids and become liquid at room temperature upon addition of small amounts of water (H_2O/IL molar ratios >1.0 or 1.5). Choline propionate is a notable exception, since it exhibits a fully liquid range either dry or hydrated down to −80 °C. Thermal analysis revealed a slight increase in the thermal stability of choline-based ILs, likely due to the enhanced cation–anion interactions through hydrogen bonding enabled by the presence of hydroxyl groups.

Among the IL hydrates tested, $[N_{1\,1\,1\,3}][AcO]\cdot H_2O$ demonstrated the highest CO_2 capture capacity, that is, 1.04 mol(CO_2)/mol(IL) at 35 °C and 3.0 ± 0.1 bar (initial pressure). The CO_2 solubility in hydrated choline carboxylate ILs was found to be lower at the same H_2O/IL ratio compared to ionic liquids containing the same anion but lacking hydroxyl groups in the cation. Notwithstanding this, the wider liquid range of choline propionate at lower hydration degrees enables high CO_2 solubility, reaching 0.7 mol(CO_2)/mol(IL) for $[N_{1\,1\,1\,2OH}][Pro]\cdot 0.5H_2O$. Interestingly, no solids were formed for choline carboxylate hydrates ($[N_{1\,1\,1\,2OH}][AcO]\cdot xH_2O$ or $[N_{1\,1\,1\,2OH}][Pro]\cdot xH_2O$) after CO_2 uptake, whilst solid bicarbonates or carbonates precipitated from $[N_{1\,1\,1\,3}]^+$ ILs and anhydrous $[N_{1\,1\,1\,2OH}][Pro]$, respectively. This was suggested by NMR and FTIR spectroscopies. Specifically for the latter case, ^{13}C NMR analysis of CO_2-saturated $[N_{1\,1\,1\,2OH}][Pro]$ revealed two new peaks around 155 ppm and 160 ppm. The peak at around 155 ppm suggests the formation of an organic carbonate *via* the nucleophilic attack of the hydroxyl oxygen atom of the choline cation on CO_2, indicating the involvement of the choline-based cation in the CO_2 capture process. Addition of water results in organic carbonate hydrolysis and the ensuing formation of bicarbonate. Further structural characterisation will be devoted to confirming these postulated mechanistic routes.

Data availability

The data supporting this article have been included as part of the ESI.†

Author contributions

Mohammad Yousefe: conceptualization, data curation, formal analysis, investigation, methodology, writing – original draft; Katarzyna Glińska: investigation, methodology, validation, visualization; Michael Sweeney: investigation, methodology; Leila Moura: data curation, formal analysis, resources, supervision, validation; Małgorzata Swadźba-Kwaśny: formal analysis, project administration, resources, supervision, validation, writing – review & editing; Alberto Puga: conceptualization, data curation, formal analysis, funding acquisition, investigation, methodology, project administration, resources, supervision, validation, writing – review & editing.

Conflicts of interest

There are no conflicts to declare.

Acknowledgements

This work is part of the CNS2023-143686 and PID2020-116322RB-C32 projects, funded by the Spanish Research State Agency (Agencia Estatal de Investigación, AEI/10.13039/501100011033). M. Y., K. G. and A. P. thank Generalitat de Catalunya, Agència de Gestió d'Ajuts Universitaris i de Recerca for grant 2021 SGR 00033. We thank Dr Rudra Purusottam for acquisition of solid-state NMR data at the School of Chemistry and Chemical Engineering, Queen's University Belfast. The instrument was funded by Engineering and Physical Sciences Research Council (EPSRC). The Universitat Rovira i Virgili team thanks Coca-Cola Europacific Partners for its financial support of the ongoing research.

References

1 M. Erans, E. S. Sanz-Pérez, D. P. Hanak, Z. Clulow, D. M. Reiner and G. A. Mutch, *Energy Environ. Sci.*, 2022, **15**, 1360–1405.
2 J. Cresko, E. Rightor, A. Carpenter, K. Peretti, N. Elliott, S. Nimbalkar, W. Morrow III, A. Hasanbeigi, B. Hedman, S. Supekar, C. McMillan, A. Hoffmeister, A. Whitlock, T. Igogo, J. Walzberg, C. D'Alessandro, S. Andersen, S. Atnoorkar, S. Upsani, P. K. Grgich, L. Ovard, R. Foist, A. Conner, M. Meshek, A. Hicks, C. Dollinger and H. Liddell, US Department of Energy's Industrial Decarbonization Roadmap, *USDOE Office of Energy Efficiency and Renewable Energy*, EERE, 2022, DOE/EE-2635.
3 R. R. Bottoms, Separating Acid Gases, *US Pat.* 1783901, 1930.
4 G. T. Rochelle, *Science*, 2009, **325**, 1652–1654.
5 E. I. Koytsoumpa, C. Bergins and E. Kakaras, *J. Supercrit. Fluids*, 2018, **132**, 3–16.

6 G. Rochelle, E. Chen, S. Freeman, D. Van Wagener, Q. Xu and A. Voice, *Chem. Eng. J.*, 2011, **171**, 725–733.
7 A. S. Babu and G. T. Rochelle, *Int. J. Greenhouse Gas Control*, 2022, **113**, 103531.
8 C. Tsay, R. C. Pattison, Y. Zhang, G. T. Rochelle and M. Baldea, *Appl. Energy*, 2019, **252**, 113379.
9 T. Gao and G. T. Rochelle, *Ind. Eng. Chem. Res.*, 2019, **59**, 7174–7181.
10 M. E. Boot-Handford, J. C. Abanades, E. J. Anthony, M. J. Blunt, S. Brandani, N. Mac Dowell and P. S. Fennell, *Energy Environ. Sci.*, 2014, **7**, 130–189.
11 D. Y. Leung, G. Caramanna and M. M. Maroto-Valer, *Renewable Sustainable Energy Rev.*, 2014, **39**, 426–443.
12 E. E. Ünveren, B. Ö. Monkul, Ş. Sarıoğlan, N. Karademir and E. Alper, *Petroleum*, 2017, **3**, 37–50.
13 M. A. Scheiman, A review of monoethanolamine chemistry, US Naval Research Laboratory, Surface Chemistry Branch, 1962, pp. 1–51.
14 G. Choudhary, J. Dhariwal, M. Saha, S. Trivedi, M. K. Banjare, R. Kanaoujiya and K. Behera, *Environ. Sci. Pollut. Res.*, 2024, **31**, 10296–10316.
15 B. B. Hansen, S. Spittle, B. Chen, D. Poe, Y. Zhang, J. M. Klein, A. Horton, L. Adhikari, T. Zelovich, B. W. Doherty, B. Gurkan, E. J. Maginn, A. Ragauskas, M. Dadmun, T. A. Zawodzinski, G. A. Baker, M. E. Tuckerman, R. F. Savinell and J. R. Sangoro, *Chem. Rev.*, 2020, **121**, 1232–1285.
16 G. Kaur, H. Kumar and M. Singla, *J. Mol. Liq.*, 2022, **351**, 118556.
17 C. J. Clarke, W. C. Tu, O. Levers, A. Brohl and J. P. Hallett, *Chem. Rev.*, 2018, **118**, 747–800.
18 Z. Lei, B. Chen, Y. M. Koo and D. R. MacFarlane, *Chem. Rev.*, 2017, **117**, 6633–6635.
19 J. S. Wilkes, *Green Chem.*, 2002, **4**, 73–80.
20 S. K. Singh and A. W. Savoy, *J. Mol. Liq.*, 2020, **297**, 112038.
21 J. F. Brennecke and B. E. Gurkan, *J. Phys. Chem. Lett.*, 2010, **1**, 3459–3464.
22 J. E. Bara, T. K. Carlisle, C. J. Gabriel, D. Camper, A. Finotello, D. L. Gin and R. D. Noble, *Ind. Eng. Chem. Res.*, 2009, **48**, 2739–2751.
23 S. Zeng, X. Zhang, L. Bai, X. Zhang, H. Wang, J. Wang, D. Bao, M. Li, X. Liu and S. Zhang, *Chem. Rev.*, 2017, **117**, 9625–9673.
24 M. Ramdin, T. W. de Loos and T. J. Vlugt, *Ind. Eng. Chem. Res.*, 2012, **51**, 8149–8177.
25 C. Cadena, J. L. Anthony, J. K. Shah, T. I. Morrow, J. F. Brennecke and E. J. Maginn, *J. Am. Chem. Soc.*, 2004, **126**, 5300–5308.
26 M. Hasib-ur-Rahman, M. Siaj and F. Larachi, *Chem. Eng. Process.*, 2010, **49**, 313–322.
27 M. B. Shiflett and A. Yokozeki, *Ind. Eng. Chem. Res.*, 2005, **44**, 4453–4464.
28 M. Yousefe, B. Ursano, J. A. Reina and A. Puga, *J. Environ. Manage.*, 2023, **334**, 117469.
29 K. Seo, C. Tsay, B. Hong, T. F. Edgar, M. A. Stadtherr and M. Baldea, *ACS Sustainable Chem. Eng.*, 2020, **8**, 10242–10258.
30 K. E. Gutowski and E. J. Maginn, *J. Am. Chem. Soc.*, 2008, **130**, 14690–14704.
31 M. B. Glier, T. J. Green and A. M. Devlin, *Mol. Nutr. Food Res.*, 2014, **58**, 172–182.
32 S. Aparicio and M. Atilhan, *J. Phys. Chem. B*, 2012, **116**, 9171–9185.
33 S. Aparicio, M. Atilhan, M. Khraisheh and R. Alcalde, *J. Phys. Chem. B*, 2011, **115**, 12473–12486.
34 S. Aparicio, M. Atilhan, M. Khraisheh, R. Alcalde and J. Fernandez, *J. Phys. Chem. B*, 2011, **115**, 12487–12498.
35 S. Bazhenov, M. Ramdin, A. Volkov, V. Volkov, T. J. Vlugt and T. W. de Loos, *J. Chem. Eng. Data*, 2014, **59**, 702–708.
36 X. Yuan, S. Zhang, J. Liu and X. Lu, *Fluid Phase Equilib.*, 2007, **257**, 195–200.
37 K. A. Kurnia, C. D. Wilfred and T. Murugesan, *J. Chem. Thermodyn.*, 2009, **41**, 517–521.
38 A. Pinkert, K. L. Ang, K. N. Marsh and S. Pang, *Phys. Chem. Chem. Phys.*, 2011, **13**, 5136–5143.
39 B. L. Gadilohar and G. S. Shankarling, *J. Mol. Liq.*, 2017, **227**, 234–261.
40 S. Bhattacharyya, A. Filippov and F. U. Shah, *Phys. Chem. Chem. Phys.*, 2017, **19**, 31216–31226.
41 M. B. Shiflett, D. W. Drew, R. A. Cantini and A. Yokozeki, *Energy Fuels*, 2010, **24**, 5781–5789.
42 A. Yokozeki, M. B. Shiflett, C. P. Junk, L. M. Grieco and T. Foo, *J. Phys. Chem. B*, 2008, **112**, 16654–16663.
43 J. Avila, L. F. Lepre, C. C. Santini, M. Tiano, S. Denis-Quanquin, K. Chung Szeto, A. A. H. Padua and M. Costa Gomes, *Angew. Chem.*, 2021, **133**, 12986–12992.
44 A. Puga, M. Yousefe, K. Glińska, R. Garcia-Valls and M. Giamberini, *Sep. Purif. Technol.*, 2025, **354**, 128443.
45 K. Anderson, M. P. Atkins, J. Estager, Y. Kuah, S. Ng, A. A. Oliferenko, N. V. Plechkova, A. V. Puga, K. R. Seddon and D. F. Wassell, *Green Chem.*, 2015, **17**, 4340–4354.
46 S. Stevanovic, A. Podgorsek, L. Moura, C. C. Santini, A. A. Padua and M. C. Gomes, *Int. J. Greenhouse Gas Control*, 2013, **17**, 78–88.
47 G. Wang, W. Hou, F. Xiao, J. Geng, Y. Wu and Z. Zhang, *J. Chem. Eng. Data*, 2011, **56**, 1125–1133.
48 G. N. Wang, Y. Dai, X. B. Hu, F. Xiao, Y. T. Wu, Z. B. Zhang and Z. Zhou, *J. Mol. Liq.*, 2012, **168**, 17–20.
49 G. Gurau, H. Rodríguez, S. P. Kelley, P. Janiczek, R. S. Kalb and R. D. Rogers, *Angew. Chem., Int. Ed.*, 2011, **50**, 12024.
50 Y. Yasaka, M. Ueno and Y. Kimura, *Chem. Lett.*, 2014, **43**, 626–628.
51 Y. Yasaka and Y. Kimura, *J. Chem. Eng. Data*, 2016, **61**, 837–845.
52 R. Quinn, J. B. Appleby and G. P. Pez, *J. Am. Chem. Soc.*, 1995, **117**, 329–335.
53 J. L. Ferguson, J. D. Holbrey, S. Ng, N. V. Plechkova, K. R. Seddon, A. A. Tomaszowska and D. F. Wassell, *Pure Appl. Chem.*, 2011, **84**, 723–744.
54 J. B. Edson, C. S. Macomber, B. S. Pivovar and J. M. Boncella, *J. Membr. Sci.*, 2012, **399**, 49–59.
55 J. M. Young, S. H. Mccalmont, S. Fourmentin, P. Manesiotis, J. D. Holbrey and L. Moura, *ACS Sustainable Chem. Eng.*, 2023, **11**, 17787–17796.

56 N. Muhammad, M. I. Hossain, Z. Man, M. El-Harbawi, M. A. Bustam, Y. A. Noaman, N. B. M. Alitheen, M. K. Ng, G. Hefter and C. Y. Yin, *J. Chem. Eng. Data*, 2012, **57**, 2191–2196.
57 Y. Fukaya, Y. Iizuka, K. Sekikawa and H. Ohno, *Green Chem.*, 2007, **9**, 1155–1157.
58 J. C. Hicks, J. H. Drese, D. J. Fauth, M. L. Gray, G. Qi and C. W. Jones, *J. Am. Chem. Soc.*, 2008, **130**, 2902–2903.
59 G. Cui, J. Wang and S. Zhang, *Chem. Soc. Rev.*, 2016, **45**, 4307–4339.
60 D. J. Yeadon, J. Jacquemin, N. V. Plechkova, M. Maréchal and K. R. Seddon, *ChemPhysChem*, 2020, **21**, 1369–1374.
61 D. J. Heldebrant, P. K. Koech, M. T. C. Ang, C. Liang, J. E. Rainbolt, C. R. Yonker and P. G. Jessop, *Green Chem.*, 2010, **12**, 713–721.